

Article

DC Bus Voltage Stabilization and SOC Management Using Optimal Tuning of Controllers for Supercapacitor Based PV Hybrid Energy Storage System

Saswati Pattnaik¹, Mano Ranjan Kumar^{1,*}, Sunil Kumar Mishra¹, Shivam Prakash Gautam¹, Bhargav Appasani¹ and Taha Selim Ustun^{2,*}

¹ School of Electronics Engineering, KIIT University, Bhubaneswar 751024, Odisha, India

² Fukushima Renewable Energy Institute, AIST (FREIA), Koriyama 963-0298, Japan

* Correspondence: mano.kumarfet@kiit.ac.in (M.R.K.); selim.ustun@aist.go.jp (T.S.U.)

Abstract: The global initiative of decarbonization has led to the popularity of renewable energy sources, especially solar photovoltaic (PV) cells and energy storage systems. However, standalone battery-based energy storage systems are inefficient in terms of the shelf and cycle life, reliability, and overall performance, especially in instantaneous variations in solar irradiance and load. In order to overcome this, a combination of a supercapacitor and battery-based hybrid energy storage system (HESS) is considered as an emerging and viable solution. The present work proposes an optimally tuned tilt-integral (TI) controller to develop an efficient power management strategy (PMS) to enhance the overall system performance. The controller parameters are tuned by optimization of the time-domain design specifications using a gradient-free simplex search technique. The robustness of the proposed TI controller is demonstrated in comparison to PI and fractional-order PI (FOPI) controllers. Furthermore, extensive experimentation was carried out to analyze the effectiveness of the proposed approach for DC bus voltage stabilization and state-of-charge (SOC) management under varying operating conditions such as solar irradiance, load, temperature, and SOC consumption by battery.

Keywords: photovoltaic; batteries; supercapacitor; SOC consumption; DC bus voltage stabilization; PI controller; fractional order PI controller; tilt-integral controller



Citation: Pattnaik, S.; Kumar, M.R.; Mishra, S.K.; Gautam, S.P.; Appasani, B.; Ustun, T.S. DC Bus Voltage Stabilization and SOC Management Using Optimal Tuning of Controllers for Supercapacitor Based PV Hybrid Energy Storage System. *Batteries* **2022**, *8*, 186. <https://doi.org/10.3390/batteries8100186>

Academic Editors: Juan Carlos Álvarez Antón, David Anseán and Matthieu Dubarry

Received: 22 July 2022

Accepted: 11 October 2022

Published: 15 October 2022

Publisher's Note: MDPI stays neutral with regard to jurisdictional claims in published maps and institutional affiliations.



Copyright: © 2022 by the authors. Licensee MDPI, Basel, Switzerland. This article is an open access article distributed under the terms and conditions of the Creative Commons Attribution (CC BY) license (<https://creativecommons.org/licenses/by/4.0/>).

1. Introduction

The unprecedented industrialization and increased energy demand have resulted in a drastic rise in global warming in the recent past. Fossil fuel (coal, oil, and gas)-based energy generation is the largest source of global emissions of greenhouse gases. Therefore, modern energy demands are leaning toward renewable energy technologies that can create sustainable and environmentally friendly energy. These technologies, if utilized effectively, can meet a significant share of the global energy demands, improve the environmental condition, and contribute to a strong energy economy. The most well-known renewable energy sources are solar [1], wind [2], biomass [3], thermal [4], ocean waves [5], and hydro [6]. Solar photovoltaic (PV) technology is the most prevalent renewable source due to its cost-effectiveness [7] and easy installation compared to its other counterparts [8]. However, the unpredictable nature of these energy sources can lead to irregular energy supply patterns. Therefore, the integration of a PV system with an energy storage system is necessary for assuring the harvested energy's reliability [9]. Batteries are considered the most preferable choice for storing electrical energy, and there has been an exponential growth in battery technology in terms of research advancements and their applications [10,11]. However, a standalone battery-based energy storage system struggles in the case of instantaneous peak power demand due to its relatively low specific power density. Because of this, different energy storage devices are employed to develop a hybrid energy storage system

(HESS) that provides a sustainable and reliable overall performance by compensating for their drawbacks and exploiting respective benefits [12–14]. Among others, supercapacitor and battery-based HESS are witnessing widespread popularity to support and meet the energy demands in the long run [15], where batteries accomplish energy requirements for a relatively long duration and supercapacitors are used to meet the instantaneous power demands and sustain a high input current. This is attributed to the fact that supercapacitors have a relatively high specific power density, higher rate of charging–discharging, and low equivalent series resistance (ESR), resulting in extremely low or negligible leakage current, resulting in superior energy retention [16,17].

A range of control and energy management strategies for PV systems with battery-supercapacitor-based HESS were reported in [18–22]. These are classified into two major categories: classical [18] and intelligent control techniques [22]. Classical methods (i.e., rule-based and filtration-based controllers) require an accurate system model and are sensitive to model parameter variations. In contrast, intelligent methods (i.e., fuzzy logic and artificial neural network-based controllers) are known to be robust and adaptive to the system parameters [23]. However, the same fails to provide optimal and efficient system performance. Therefore, to avoid the impact of model parameter variations and ensure efficient performance, optimized and predictive control techniques are adopted for HESS [20]. Model predictive control (MPC) [16] and simple PI control [15] based strategies were proposed for HESS, which improves the lifespan of the battery by diverting the power surges to the supercapacitor and associated charge–discharge current regulations. Although the MPC helps predict future system behavior and can optimize the system performance, it suffers from computational complexity and is intensive [14]. In [22], different optimization algorithm-based tuning of the PI controller was analyzed for the robust and efficient performance of HESS, and the particle swarm optimization (PSO) technique was found to outperform among the others. However, the computational complexity of the PSO was not taken into account.

Furthermore, simple PI controllers are not suitable for nonlinear systems such as electrochemical batteries and supercapacitor-based HESS. Electrochemical systems are known for their unusual fractional-order behavior due to the diffusion and migration of ions within the porous electrode and electrolyte interface [24–26]. To address a nonlinear system's requirements, fractional-order controllers are often used for their robust performance during parameter variations [27]. A tilted-integral differential (TID) controller is a type of fractional-order controller, considered to be an extension of conventional integer-order PID controller, that can be easily tuned, and if optimally tuned, it can outperform the PID controllers in terms of robustness with respect to external disturbances and system parameter variations [28]. Several investigators have proposed the efficient control capability of TID cascaded with PID for enhanced performance but with less emphasis on DC bus voltage regulation. However, it is emphasized for load frequency control in power system applications [29,30]. The authors in [31] recently proposed a standalone hybrid energy system using the optimal TID controller for voltage regulation for a PV-integrated battery bank with AC load and not with an integrated battery and supercapacitor-based PV-HESS with DC load.

Considering the instantaneous variation of the input conditions such as irradiance and temperature, there is a need to secure the stability of the system. Additionally, there is a need to improve the condition of the battery by reducing its state-of-charge (SOC) consumption. Although the reported works in this direction have focused on the concept from several dimensions, less attention has been given to an optimally tuned efficient but simple fractional-order controller for DC bus voltage for PV-integrated HESS with SOC management. The aim of the paper was to design an optimally tuned fractional-order TI controller for DC bus voltage stabilization and demonstrate the potential benefits of the supercapacitor in further refining the HESS performance by emphasizing the power management between the PV source, battery, and supercapacitor. Further study was carried out with performance analysis of the system with variable input and load conditions and

using those parameters to check the amount of SOC consumed in the batteries. These simulation studies were carried out to assess the performance of the proposed power management strategy so that it was robust enough to adapt to different input conditions without affecting the battery lifetime.

The main contributions of the proposed work are:

- A novel TI control scheme is proposed for the DC bus voltage stabilization of the battery and supercapacitor-based HESS.
- Its performance was compared with that of integer-order PI and fractional-order PI controllers to demonstrate the feasibility of the proposed TI controller.
- To present the robustness of the proposed controller by subjecting it to varying input (irradiance and temperature) and load conditions.
- To estimate the amount of SOC consumed in the battery under varying temperature conditions and determine the effectiveness of the controller performance in reducing stress on the battery.

The rest of this manuscript is organized as follows. Section 2 describes the modeling and system configuration along with the schematic representation of the standalone PV system under study. Section 3 presents the proposed control scheme, and Section 4 depicts the simulation results and validation with different case studies and their analysis. Finally, the concluding remarks of the research work are summarized in Section 5.

2. Modeling and System Configuration

Battery and supercapacitor-based HESS has an extra edge over the standalone battery-based ESS for different renewable energy sources, and a grid-free PV-based system is no exception [32,33]. These HESS can be built by batteries and supercapacitors configured in different topologies. Table 1 lists some of the most popular topologies of battery-supercapacitor-based HESS along with their properties. The standalone PV system under study uses the multiple converter topology, as shown in Figure 1. It consists of a solar PV system connected to the DC bus through a boost converter and maximum power point tracking (MPPT) controller (by P&O method [34]) to extract the maximum power from PV. The energy storage system under investigation consists of a battery and a supercapacitor connected to the DC bus via buck–boost converters. Hence, the entire system is mainly comprised of three sources:

- A PV panel is the main source of energy.
- A battery is used in the case of a surplus/deficiency of energy harvesting from the PV system.
- A supercapacitor limits the PV/load variation and assists the battery in the case of sudden fluctuations.

PV cells or solar cells are the core components of all PV systems as they convert Sun radiation to electrical energy. Figure 2 depicts a solar cell's practical circuit model consisting of a diode, series resistance, and parallel resistance. The V–I characteristic equation of a solar cell is given by:

$$I = I_{pv} - I_s \left[\exp \left(\left(\frac{qV + IR_s}{KT_c A} \right) - 1 \right) - \left(\frac{V + IR_s}{R_p} \right) \right] \quad (1)$$

where I_{pv} is the solar current; I_s is the cell saturation current; q is the electron charge; K is the Boltzmann constant; T_c is the cell working temperature; A is the ideality factor.

Table 1. Different system configurations.

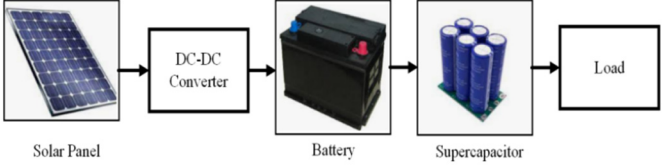
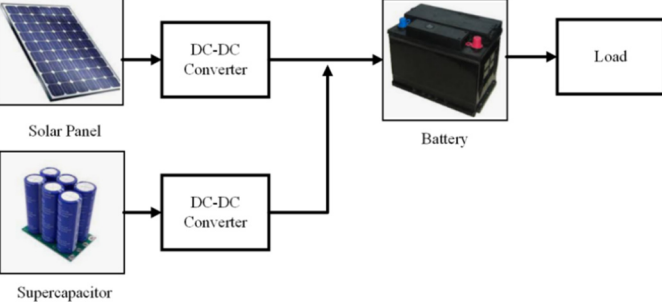
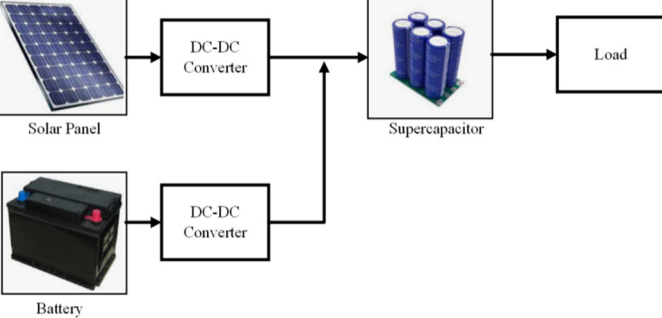
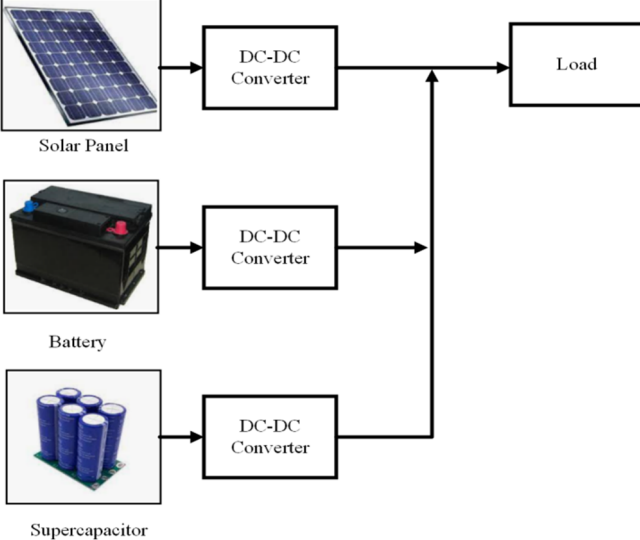
| Configuration | Topology | Features | Drawback |
|---|--|--|--|
| Basic passive parallel Hybrid configuration |  <p>The diagram shows a solar panel connected to a DC-DC converter. The output of the converter is connected to a battery and a supercapacitor in parallel, which then feeds into a load.</p> | <p>Supercapacitor and battery are directly connected with load. Hence it is easy to implement with good reliability</p> | <p>Power sharing between battery and supercapacitor is uncontrolled. Hence the DC bus voltage is not regulated</p> |
| Supercapacitor/battery parallel configuration |  <p>The diagram shows a solar panel and a supercapacitor, each connected to its own DC-DC converter. The outputs of both converters are connected to a battery, which then feeds into a load.</p> | <p>Supercapacitor energy is used more efficiently to maintain constant DC bus voltage that changes w.r.t SOC of battery</p> | <p>DC Bus voltage regulation is difficult to obtain and there are chances of load imbalance</p> |
| Battery/supercapacitor parallel configuration |  <p>The diagram shows a solar panel and a battery, each connected to its own DC-DC converter. The outputs of both converters are connected to a supercapacitor, which then feeds into a load.</p> | <p>Battery voltage can be higher and lower than the supercapacitor voltage. It costs less with a reduction in complexity due to a single converter used.</p> | <p>Improper DC bus voltage regulation due to the supercapacitor variable voltage</p> |

Table 1. Cont.

| Configuration | Topology | Features | Drawback |
|--------------------|--|--|--|
| Multiple converter |  <p>The diagram illustrates a multiple converter topology. On the left, three energy sources are listed vertically: a Solar Panel (represented by a blue grid icon), a Battery (represented by a black battery icon), and a Supercapacitor (represented by four blue cylindrical icons). Each source is connected to a separate DC-DC Converter box. Arrows from each of these three converter boxes point towards a central vertical line. From the top of this line, an arrow points to a Load box on the right.</p> | <p>Most efficient configuration is a separate converter for the battery and a supercapacitor is used, which provides the easy control of power</p> | <p>High cost due to complex circuitry and a large number of components</p> |

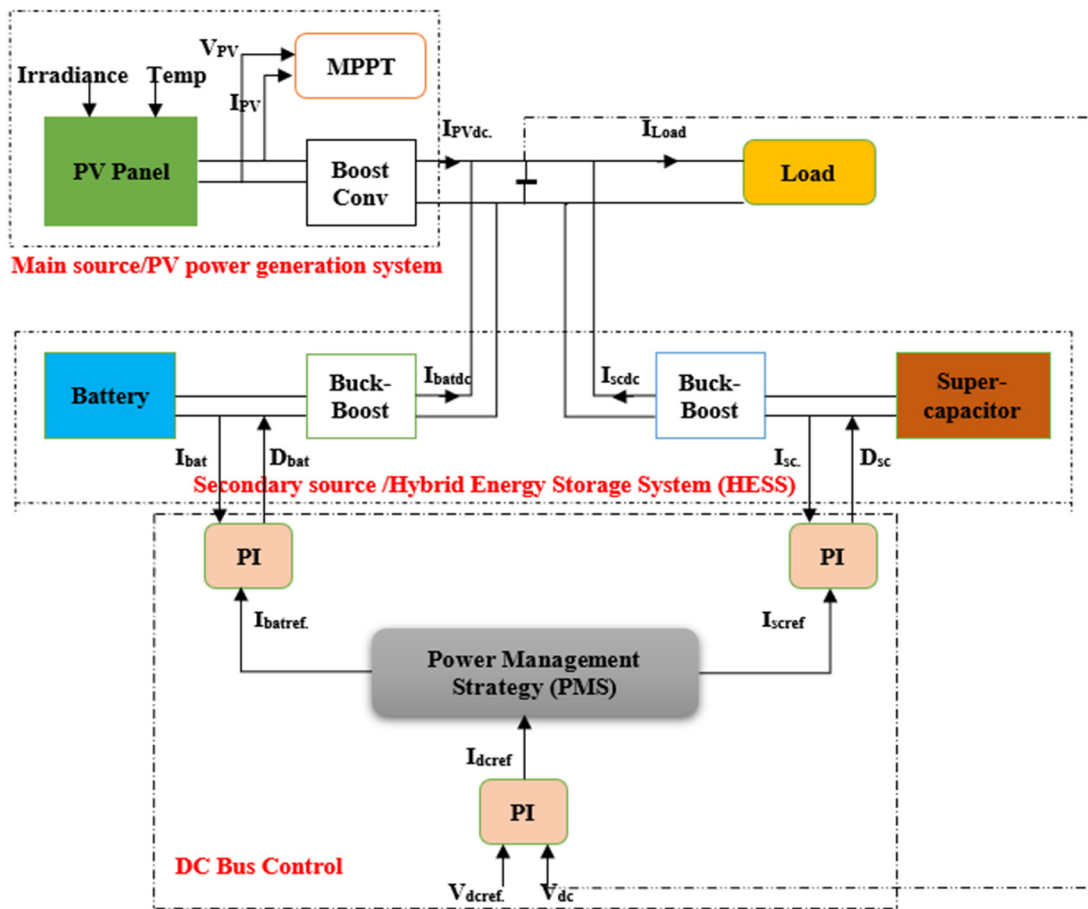


Figure 1. Schematic diagram of the PV system with the energy storage devices.

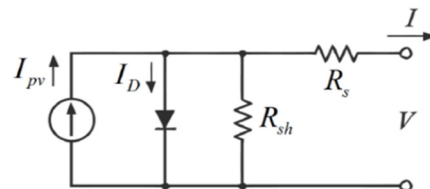


Figure 2. Equivalent circuit model of a PV cell.

A solar panel or PV panel is a collection of these solar cells electrically wired together with parallel and series connections. In this case, the load current I with N_P parallels and N_S series modules is denoted as,

$$I = N_P I_{pv} - N_P I_s \left[\exp \left(q \left(\frac{V}{N_S} + \frac{I R_s}{N_P} \right) \frac{1}{K T_c A} \right) - 1 - \left(\frac{N_P V}{N_S} + I R_s \right) \frac{1}{R_{sh}} \right] \quad (2)$$

In this case, any variation in the solar irradiance or operating temperature will directly affect the magnitude of the solar current, maximum power, and voltage. The saturation current and voltage are dependent on temperature [35]. The PV panels were connected with a boost converter to boost the output voltage and a MPPT controller using the popular P&O method to extract the maximum power from the PV panel. The batteries and supercapacitor forming the HESS are connected to the DC bus and a bidirectional buck–boost converter to maintain a two-way flow of current from PV-HESS or from HESS to PV [36]. The switching operation of these converters is controlled using a PI controller. The specifications of all parameter values used in the PV module, battery, and supercapacitor are listed below in Table 2.

Table 2. The system parameter specifications [17].

| Devices/Components | Parameters | Value |
|--------------------|---------------------------------------|---------------------------------|
| PV module | Maximum power | 120.7 W |
| | Short circuit current | 8 A |
| | Open circuit voltage | 21 V |
| | PV array sizing | 2 series and 4 parallel strings |
| Battery | Nominal voltage | 24 V |
| | Rated capacity | 14 Ah |
| | Initial SOC | 50% |
| Supercapacitor | Rated capacitance | 29 F |
| | Rated voltage | 32 V |
| | Initial voltage | 32 V |
| | No. of series and parallel capacitors | 1.1 |
| DC bus parameters | DC link capacitance | 300 μ F |
| | Power load | 500 W |
| | DC bus voltage | 50 V |

3. Proposed Control Scheme for PV Power System

As discussed in Section 1, with the aim of designing a simple but efficient and optimal controller, in this work, three different controllers (i.e., PI, FOPI and TI) were optimally tuned for the PV-HESS applications. These control structures are briefly described as follows.

3.1. PI Controller

This is mostly used in process diligence because of its easiness. There are two parameters to be optimized as seen in the structure shown in Figure 3a. However, it has severe oscillations with poor transient performance [37] and takes a greater amount of settling time. They are also not suitable for nonlinear systems. Its transfer function is given as $K_p + \frac{K_I}{s}$, where K_p and K_I are the proportional and integral gains, respectively.

3.2. FOPI Controller

The design of an energy management strategy for a battery-supercapacitor HESS is considered as a nonlinear multi-constraint optimization problem. Therefore, better results can be obtained using a fractional order controller, which gives better system performance and flexibility toward the parameter variations [38,39]. This controller consists of three tuning parameters K_p , K_I , and λ , as seen in Figure 3b. Its transfer function is given as $K_p + \frac{K_I}{s^\lambda}$. It increases the complexity for tuning but at the same time, has a remarkable performance in comparison to the integer-based controller. It is generally represented using fractional calculus [40], which deals with arbitrary non integer order derivatives and integrals.

3.3. TI Controller

TI is an extension of the fractional order controller [29], which consists of a proportional and integral gain with tilted components of transfer function $\frac{1}{s^{-n}}$. The inclined behavior gives a feedback gain based on frequency, which is inclined in comparison to the normal compensator's gain/frequency. This controller is simpler to design and less affected by the parameter variations [30]. The transfer function of the TI controller is expressed as $\frac{K_p}{s^{-n}} + \frac{K_I}{s}$. Figure 3c shows the structure of a TI controller.

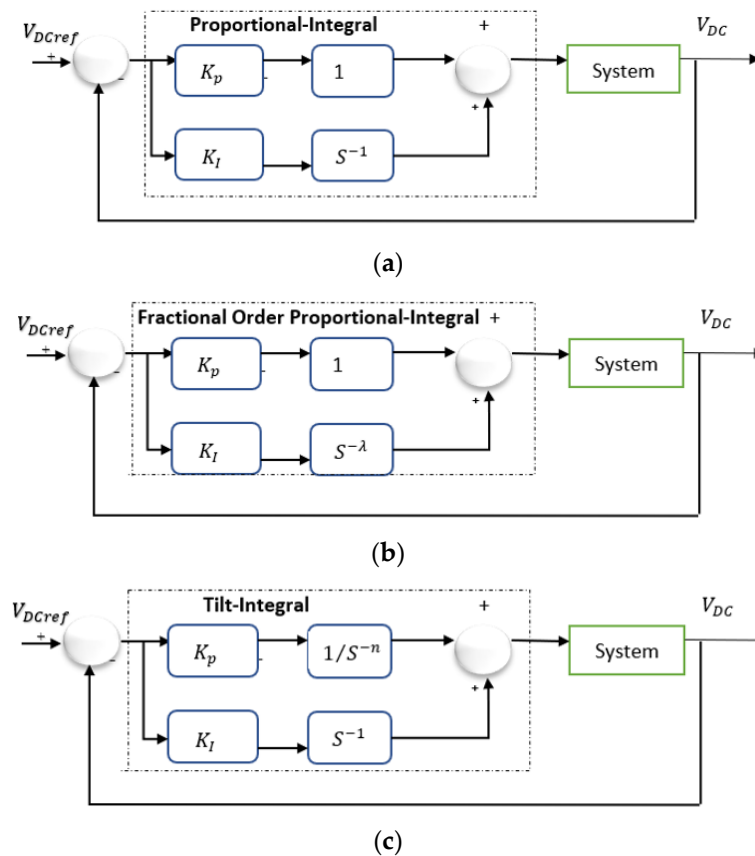


Figure 3. Block diagram of the (a) PI controller, (b) FOPI controller, and (c) TI controller.

3.4. Control Strategy to Stabilize the DC Bus Voltage

The TI controller calculates the I_{dcref} to maintain the DC bus voltage at V_{dcref} (50 V) and the same is depicted in Figure 4. The power management strategy is based on the DC bus regulation in which the battery and supercapacitor currents I_{batref} and I_{scref} are produced by the DC bus reference current I_{dcref} , which is given by:

$$I_{dcref} = I_{batref} + I_{scref} \tag{3}$$

The error between the reference voltage and actual voltage, $e(t)$ is as given as:

$$e(t) = V_{dcref} - V_{dc} \tag{4}$$

and therefore, the output for the PI controller is

$$I_{dcref} = k_p e(t) + k_i \int e(t) dt \tag{5}$$

The reference current of batteries is formed from the low pass filter that filters out the low-frequency components for the battery and the remaining high-frequency components for the supercapacitor. As a result, the batteries are supported only for the normal energy storage purpose while the peak current demands are handled by the supercapacitor, thus improving the lifetime of the batteries.

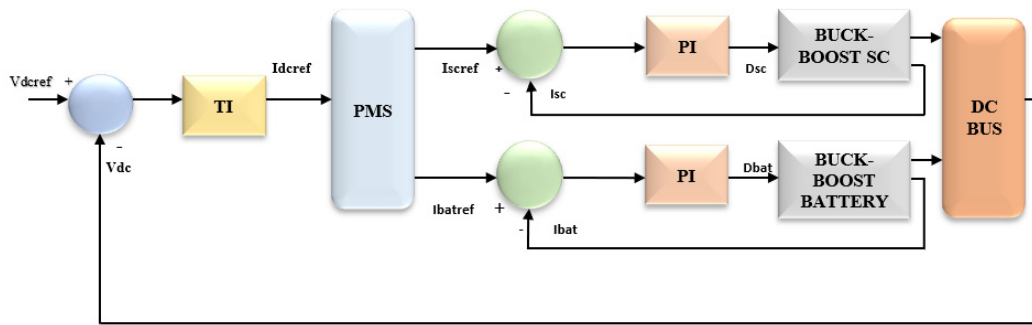


Figure 4. The proposed TI controller-based DC bus control scheme.

3.5. PMS and Control Scheme

Figure 5 shows the PMS implementation for PV-HESS using the TI control scheme. The supercapacitor is completely charged and only available for discharging when the PV power is not sufficient for the immediate load demand ($P_{pv} < P_{load}$) and the battery’s SOC is low. Similarly, the supercapacitor begins to charge when the load power is suitable to be accomplished by the PV ($P_{pv} > P_{load}$), and batteries cannot store the surplus amount of power in that short duration. Although a supercapacitor acts as a secondary storage device, it plays a pivotal role in an efficient and smooth operation of the entire PV-HESS under varying input conditions. As previously discussed, PV systems are subjected to variable irradiance and temperature at different time intervals, and the PMS used in the control block aims at reducing the stress on the battery due to continuous charging/discharging and hence improves its lifetime, stabilizing the DC voltage and attaining a better efficiency of the system under varying operating conditions [41]. Therefore, the current distribution among the battery and supercapacitor (i.e., I_{bat} and I_{sc} , respectively) constitutes the total current to be delivered by the HESS.

$$I = I_{bat} + I_{sc} \tag{6}$$

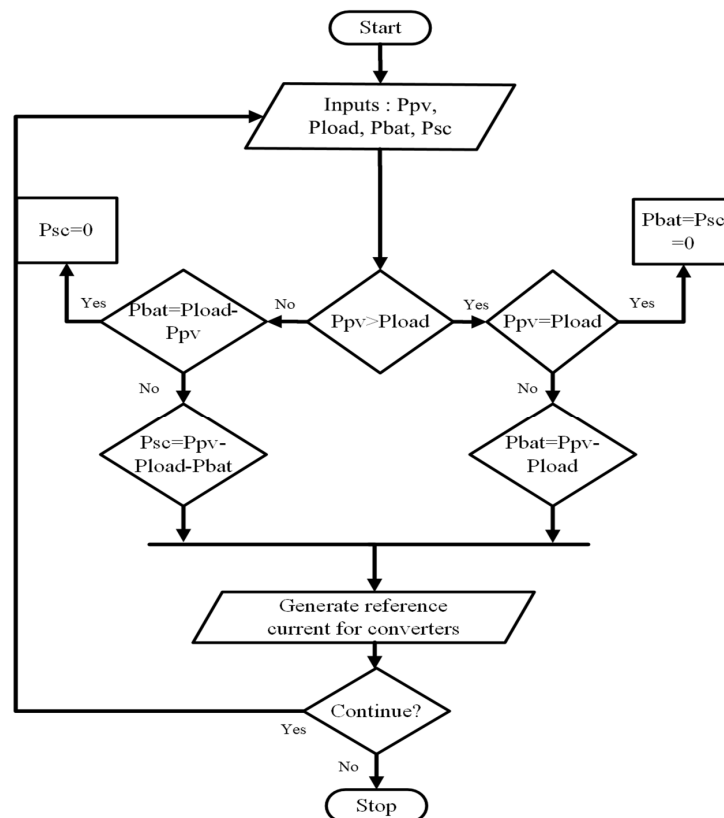


Figure 5. Power management strategy of the DC bus control.

This indicates that the current contains both high-frequency as well as low-frequency components, where the high-frequency components are associated with the supercapacitor and the low-frequency components are accompanied with the battery. For this purpose, a low-pass filter (LPF) was engaged with the circuitry. This helps the battery remain operational only for the normal charging process, while the supercapacitor handles the transient periods, involving high frequency [42], thus improving the stress on the battery and enhancing its lifetime. Therefore, the reference value of the battery current is given by

$$I_{batref} = f_{LPF}(I) \quad (7)$$

where f_{LPF} is the transfer function of a low-pass filter.

This reference value in Equation (7) was compared with the actual current value I_{bat} and this current error was given as input to the PI controller, which generates the duty cycle D_{bat} for the PWM control signal to handle the switching operation of the battery converter. However, the entire power requirement is not fulfilled by only the battery and the remaining power is compensated by the supercapacitor as

$$P_{batrem} = (I - I_{bat})V_{bat} \quad (8)$$

Thus, the reference current of the supercapacitor is given by

$$I_{scref} = \frac{P_{batrem}}{V_{sc}} = \frac{(I - I_{bat})V_{bat}}{V_{sc}} \quad (9)$$

Furthermore, similar to the operation of batteries, the reference current of the supercapacitor I_{scref} was compared with the actual current I_{sc} and the difference was transmitted to the PI controller to generate a duty cycle D_{sc} of the PWM control signal, which results in handling the switching operation of the supercapacitor converter. Therefore, in this cascaded control scheme, the TI controller was used for DC bus voltage regulation, while the PI controller handled the battery and supercapacitor switching operations involved in the PMS.

3.6. Optimization Based Controller Tuning

For the present investigation and analysis, the controller designing task was framed as an optimization problem, which aimed at the minimization of the deviation between the reference and the actual output (i.e., the error). This ensures the optimization of the transients that exist in the overall system response. The objective function has been formulated as the well-known controller performance indices in the time domain (i.e., integral absolute error):

$$IAE = \int_0^t |e(t)| dt \quad (10)$$

Integral squared error:

$$ISE = \int_0^t e^2(t) dt \quad (11)$$

Integral time absolute error:

$$ITAE = \int_0^t t \vee e(t) \vee dt \quad (12)$$

Integral time squared error:

$$ITSE = \int_0^t te^2(t) dt \quad (13)$$

It is of note that IAE and ISE are the most commonly used performance criteria in the stability analysis of control systems [43]. These are the most important time-domain integral

error performance criteria, which are obtained by evaluating the absolute and square of deviations between the actual and the reference output. Each of these represents a separate time-varying output norm that, under stable conditions, converges to zero [44]. The most common criteria for evaluating a system's performance are the rising time, settling time, overshoot, and steady-state error. However, each of these describes only one characteristic. The time integral criteria are broad and therefore, these also make it possible to compare different controller design methods and distinct controller structures [45]. Each criterion is generic, and it may be used to assess error in any sort of system, whether linear or nonlinear. These performance measurements are used to minimize the error in any feedback control system and thus keep track of errors from zero to infinity and minimize them continually.

Furthermore, for optimal tuning of the controller parameters, one of the most reliable and popular optimization techniques (i.e., the Nelder–Mead simplex search method was used for the present work). The Nelder–Mead simplex algorithm was proposed by Nelder and Mead (1965). It is one of the most popular and traditional direct search methods for multidimensional unconstrained minimization. The method is deterministic in its formulation, which minimizes a scalar-valued nonlinear function of real variables without any derivative information [46]. Initially, a new simplex is created with $n + 1$ points to explore the objective function of n inputs. Here, X_m is the average sum of all points. Then, the simplex has several methods to move ahead and denote the minimum: reflection, contraction, expansion, and shrink. X_r , X_c , and X_e are the points obtained from them, respectively, with f_r , f_c , and f_e being their associated function values. If the progress is sufficient, then a single point is substituted. This repetitive technique continues until the minimum is attained, with which the final k_p and k_i values are returned. To simulate the algorithm in MATLAB, a standard function `fminsearch()` was defined.

4. Results and Discussion

4.1. Dynamic Performance Evaluation of the Controllers

In this work, the main focus was on creating a robust energy storage system to support the load in the case of input fluctuations in the PV with the help of a suitable power management principle. In the proposed model, there is a greater chance of a lack of robustness when subjected to inaccuracies with the instantaneous changes in the system. While using the above-mentioned techniques, it may lead to large computational complexity due to its nonlinear behavior. Hence, a suitable power management principle designed using controllers generates the required duty cycle to control the converter's operation whenever required.

The PV-HESS under investigation was built in a MATLAB/Simulink environment and simulated with the PI, FOPI, and TI controllers. With the objective of DC bus voltage stabilization, the controllers were tuned using the Nelder–Mead simplex search technique to evaluate the different performance criteria in the stability analysis. Parameters of the system under investigation are listed in Table 2 for better clarity. Furthermore, in order to reduce the design complexity and provide suitable tuning of the standalone PV-HESS system, which is subjected to rapidly changing input and load conditions, in the present work, the derivative gains of the respective controllers were not considered. The DC bus voltage stabilization of the HESS using different (PI, FOPI, and TI) controllers was compared and analyzed. The controller parameters were optimized using the Nelder–Mead simplex search algorithm considering ITAE as the cost function. To avoid any dependency on the initial points, the algorithm was executed for 20 runs for all controllers considering different initial points. The mean and standard deviation of the optimally tuned controller parameters obtained for the PI, FOPI, and TI controllers along with the ITAE value are depicted in Table 3 and the corresponding performance of the controllers is illustrated with the help of the dynamic time-domain behavior of the overall system using the Nelder–Mead simplex optimization method. It was observed that the DC bus voltage response (Figure 6) of the TI controller was better than that provided by FOPI and PI with good convergence. Additionally, the proposed controller outperformed the other controllers

with the minimum overall standard deviation in the case of ITAE. Hence, we can say here that for different initial simplices, nearly about the same optima was achieved, proving its robustness. The advantage of the TI controller was demonstrated by a smooth DC bus voltage response that was less sensitive to the load power or input changes as well as a reduction in the oscillations and high frequency components. The transfer functions of the optimally tuned controllers are given as

$$G_{PI}(s) = 0.7115 + \frac{1692.2}{s} \tag{14}$$

$$G_{FOPI}(s) = 1.8 + \frac{50}{s^{0.5}} \tag{15}$$

$$G_{TI}(s) = \frac{0.9878}{s^{-2.1598}} + \frac{1031.8}{s} \tag{16}$$

Table 3. The mean and standard deviation for the optimally tuned controller parameters and the ITAE value for the PI, FOPI, and TI controllers.

| Controller | K_p | K_I | N | λ | ITAE |
|------------|----------------|-----------------|----------------|----------------|------------------|
| PI | 1.424 ± 0.3424 | 3037.9 ± 0.255 | - | - | 0.4881 ± 0.00649 |
| FOPI | 1.913 ± 0.098 | 50.908 ± 0.227 | - | 0.504 ± 0.0314 | 0.4203 ± 0.00239 |
| TI | 1.015 ± 0.173 | 1039.55 ± 0.358 | 2.558 ± 0.3155 | - | 0.3839 ± 0.00161 |

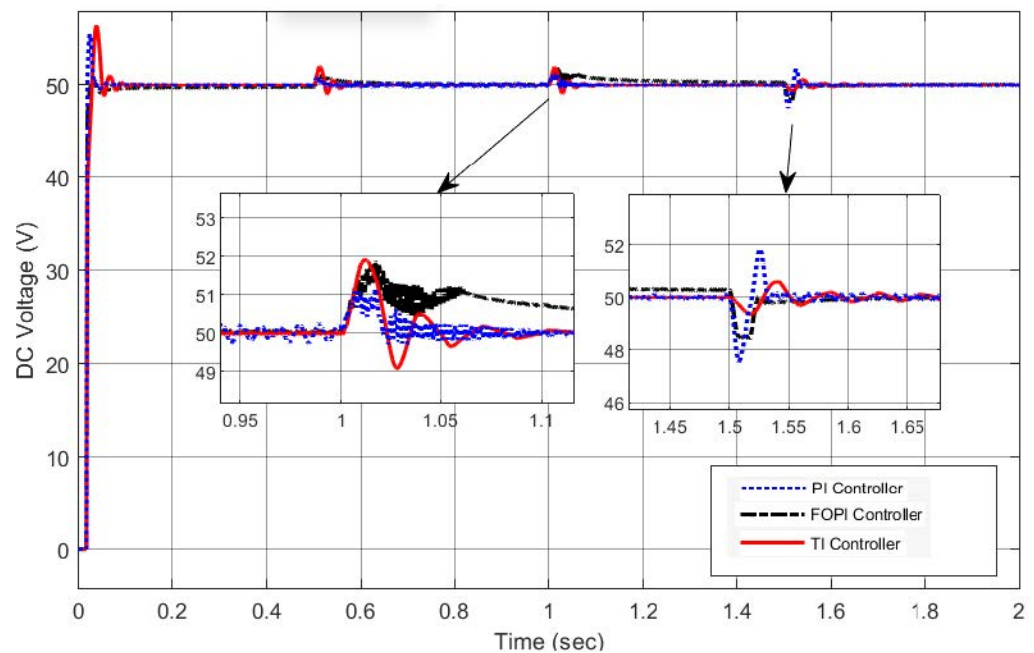


Figure 6. The DC bus voltage of the PV-HESS using the PI, FOPI, and TI controllers.

In order to compare the results with the global optimization technique, the proposed TI controller was tuned using the very popular particle swarm optimization (PSO) algorithm. PSO is an evolutionary computing method inspired by the movement of different animals such as bird flocks and fish schools. It is guided by the movement of the best member in the population, famous as the social compound, and their own experience, which is known as the cognitive compound. The algorithm moves the set of solutions to find the best solution among them [47]. Although PSO gives good results in terms of the global optimal solutions and convergence, it requires more computational time and function evaluations. As seen in Figure 7 for a fixed number of iterations/function evaluations, the value of the objective

function was not reduced in the case of PSO. In this respect, the Nelder–Mead method provides fast optimally tuned parameters for the proposed controller.

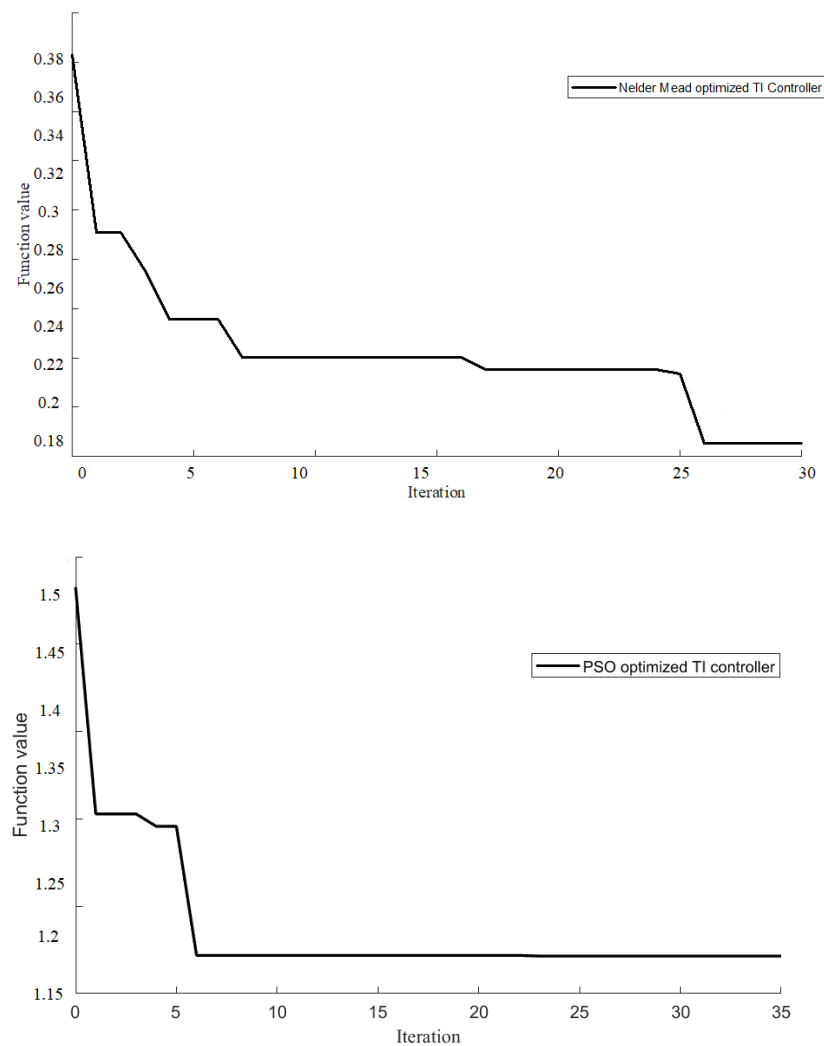


Figure 7. Optimization performance plot of the proposed TI controller using Nelder–Mead and PSO.

For better study of the stability analysis, the output response of the proposed TI controller was compared with the other controllers and this control effort performance comparison is shown in Figure 8. The results clearly show that the proposed TI controller outperformed the other controllers with reduced vibrations and fluctuations with the least estimated root mean square error (RMSE) between the actual and reference voltage. The RMSE of the control input for the PI, FOPI, and TI controllers were found to be 10.27, 7.199, and 4.705, respectively. Hence, the proposed TI controller showed a significant reduction of 54.19% and 34.64% in the control effort for both the PI and FOPI controllers, respectively.

A comparative analysis of all the controllers was also conducted in terms of the parameter specifications, namely, the settling time, undershoot and overshoot, rise time, and slew rate. Table 4 indicates that the TI controller-based system provides better results among all in terms of all of the time-domain performance criteria.

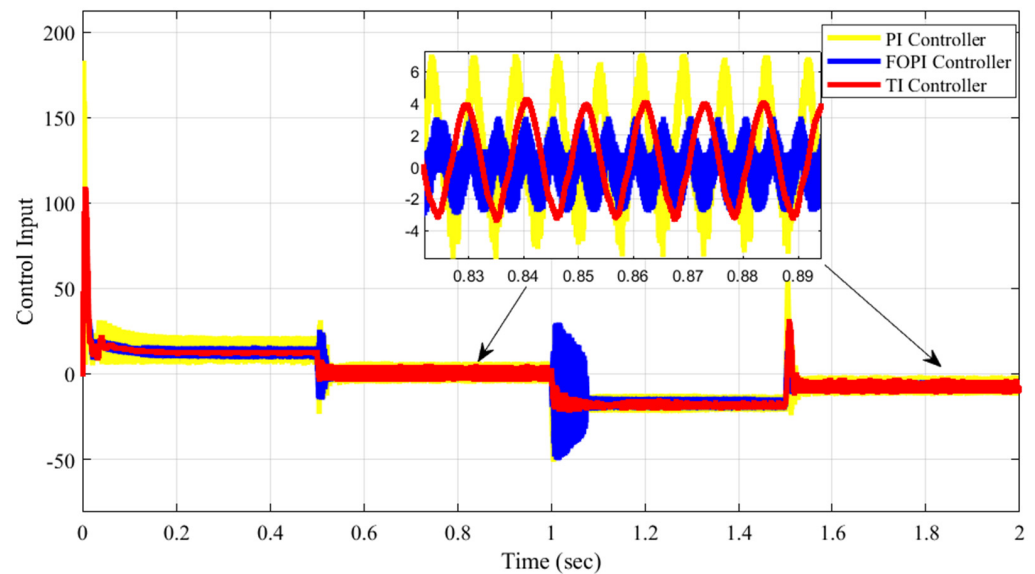


Figure 8. Control input performance of the PI, FOPI, and proposed TI controllers.

Table 4. The dynamic performance parameter comparison for the PI, FOPI, and TI controllers.

| Controller | Risetime | Undershoot (%) | Settling Time (ms) | Slew Rate |
|------------|-----------------|----------------|--------------------|-----------|
| PI | 9.410 ns | 1.340 | 9.149 | 4.229 |
| FOPI | 228.427 μ s | 1.999 | 5.691 | 173.759 |
| TI | 41.071 ps | 0.563 | 5.013 | 966.580 |

4.2. Robustness Analysis of the Proposed Controller

In this section, an extensive analysis is presented to exhibit the effectiveness of the proposed controller by considering different operating conditions such as rapid change in input solar irradiance, load conditions, and temperature. Furthermore, the estimation of SOC consumption was carried out and investigated.

4.2.1. Analysis with Varying Solar Irradiance and Load

Figure 6 shows the performance of the above PMS under variable solar irradiance input, as shown in Figure 9. From 0 to 0.5 s, $P_{pv} = 200$ W. Due to insufficient PV power, the battery also supports the load and is in discharge mode, which provides the required power. Furthermore, for the next instance (i.e., between 0.5 and 1 s,) when the power generated by PV increases from 200 W to 500 W, the PV power becomes a little insufficient to supply the load and therefore the battery discharge gradually decreases. Thereafter, during the next instance (i.e., from 1 to 1.5 s), the PV power increases from 500 W to 1000 W, the battery switches from discharging mode to charging mode, which reflects there is surplus power during this period, and a supercapacitor is also used for storage purposes. Finally, for the time instance of 1.5 to 2 s, the power produced by PV decreased from 1000 W to 700 W, and the battery switched from charging to discharging mode. However, the SOC of the battery did not reduce as the supercapacitor compensates the deficiency of power during this period.

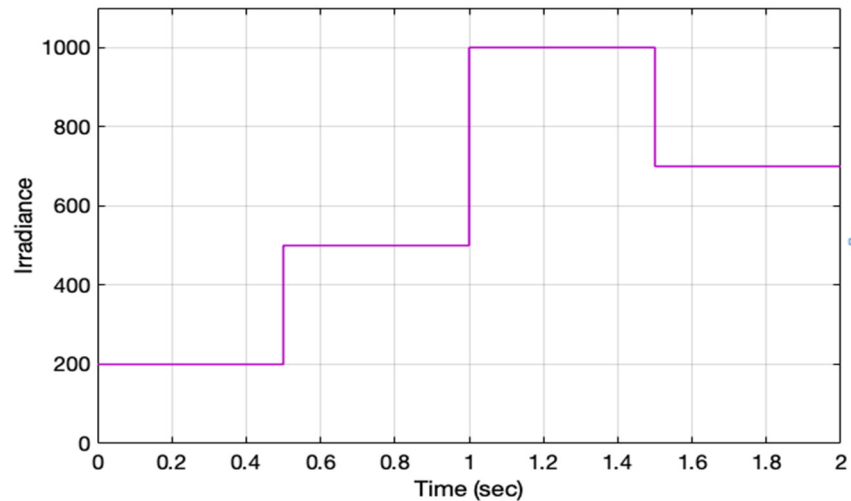


Figure 9. Variable input irradiance.

Furthermore, with the aim of investigating the robustness of the proposed control scheme under varying load conditions, the response of the battery and supercapacitor power profiles are depicted in Figures 10 and 11. This analysis was carried out using the load variation profile, the same as that of the irradiance plot. The potential benefits of the battery–supercapacitor HESS may be easily shown using the PI, FOPI, and TI controllers to improve the reactivity of the supercapacitor while charging and discharging, thus reducing the battery stress dramatically. For instance, at 0.5 s, the load increased from 200 W to 500 W, then the battery and supercapacitor started charging during this short period of time. When the load increased further to 1000 W, at that time, the battery switched from the charged state to the discharge state and the supercapacitor compensates for any lack of power. Hence, the results show the effective performance of the TI controller-based system over the others.

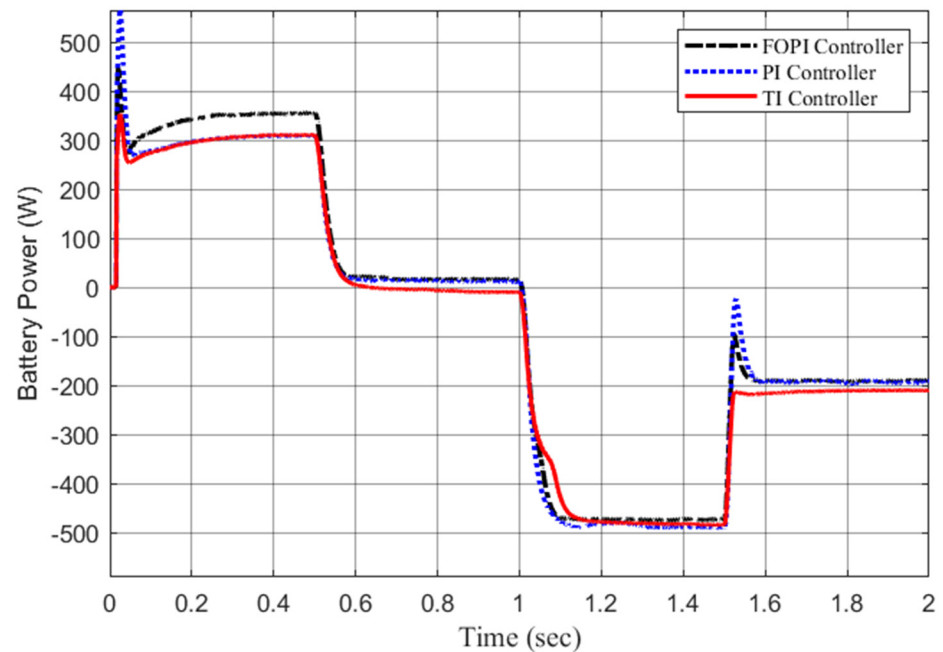


Figure 10. Response of battery power with varying irradiance and load conditions.

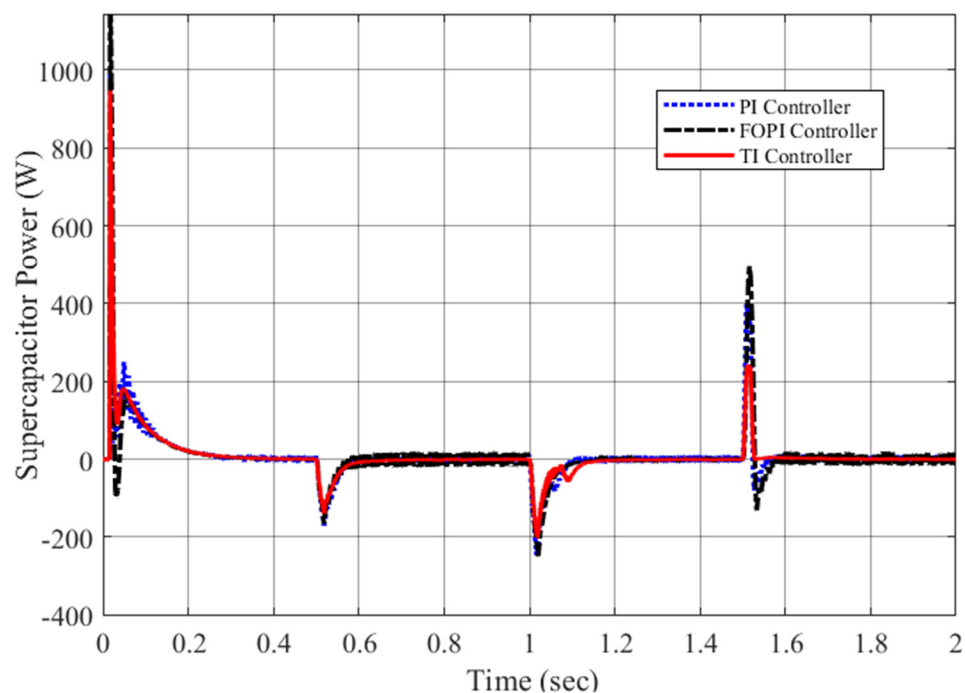


Figure 11. Response of the supercapacitor power with varying irradiance and load conditions.

4.2.2. Analysis with Varying Temperature and Estimating the SOC Consumption

As reported in [16], the SOC consumption in batteries is estimated with a change in the time constant, which is a suitable characteristic of the filter circuit. With the aim of further investigating the efficacy and robustness of the PV-HESS, here, we considered the practical scenario, which is the change in weather conditions. At first, Figure 12 shows the battery SOC of the system under the PI, FOPI, and TI controllers at room temperature (i.e., 25 °C). The comparative study validates that the SOC consumption of batteries using the TI controller is better than its other counterparts. Based on different optimal controller parameters, a comparative analysis was carried out by simulating the system for 2 s. Under different operating temperatures (i.e., 40, 25, 10, 0, −12 °C). The minimum value of SOC obtained in each case was determined for the respective controllers and the same is presented in Table 5. It was noted that the TI controller outperformed other controllers under any given temperature. Furthermore, the approximate SOC consumption of batteries for one hour was estimated by keeping a similar temperature and irradiance pattern, which highlights the importance of SOC in the long-term. Additionally, Figure 13 shows the responses of the battery SOC under different temperatures with the TI controller. It was noted that the SOC_{bat} decreased with an increase in temperature.

In this PV-HESS model, no charging strategy for the supercapacitor was considered during the energy management operation. It is completely charged and is only available for discharge when the PV power is insufficient for load and the battery SOC is less. Therefore, in the case of a reduction in the battery SOC than required, the dependency on the supercapacitor will increase. Batteries are used to store energy for higher amounts while supercapacitors have a high power density and are used to store and release power at a relatively higher rate. Therefore, to obtain a stable response irrespective of the system subjected to abrupt transient states, the supercapacitor plays an important role. Figure 14 shows the SOC consumption of the battery when the supercapacitor is not integrated along with the battery in the hybrid system. It was observed that the battery SOC decreased at a greater rate, thus increasing the stress on the battery. On the other hand, whenever a supercapacitor is used along with the battery, the rate of decrease in SOC is controlled and it does not decrease rapidly. Thus, integrating a supercapacitor with batteries reduces the battery SOC consumption by eliminating the peak currents.

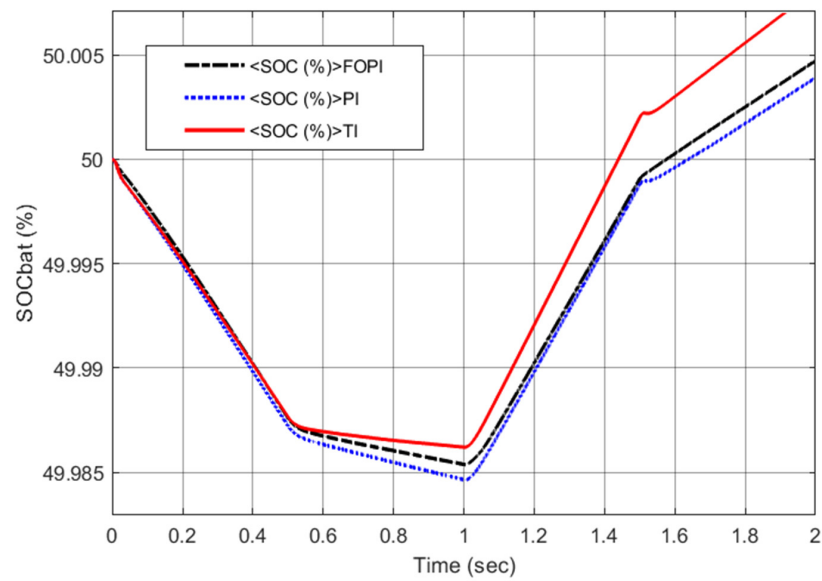


Figure 12. SOC_{bat} in the PV system with a supercapacitor for the PI, FOPI, and TI controllers.

Table 5. Consumption of SOC_{bat} for the PI, FOPI, and TI controllers.

| Case Study | Temp | Consumption of SOC | % Consumption of SOC in 1 h |
|------------|--------|--------------------|-----------------------------|
| PI | 40 °C | 0.0164 | 29.52 |
| | 25 °C | 0.0146 | 26.28 |
| | 10 °C | 0.0130 | 22.40 |
| | 0 °C | 0.0122 | 21.96 |
| | −12 °C | 0.0118 | 21.24 |
| FOPI | 40 °C | 0.0158 | 28.44 |
| | 25 °C | 0.0131 | 23.58 |
| | 10 °C | 0.0130 | 23.4 |
| | 0 °C | 0.0092 | 16.56 |
| | −12 °C | 0.009 | 16.38 |
| TI | 40 °C | 0.0149 | 26.82 |
| | 25 °C | 0.0120 | 21.60 |
| | 10 °C | 0.0109 | 19.76 |
| | 0 °C | 0.0091 | 16.38 |
| | −12 °C | 0.0088 | 15.84 |

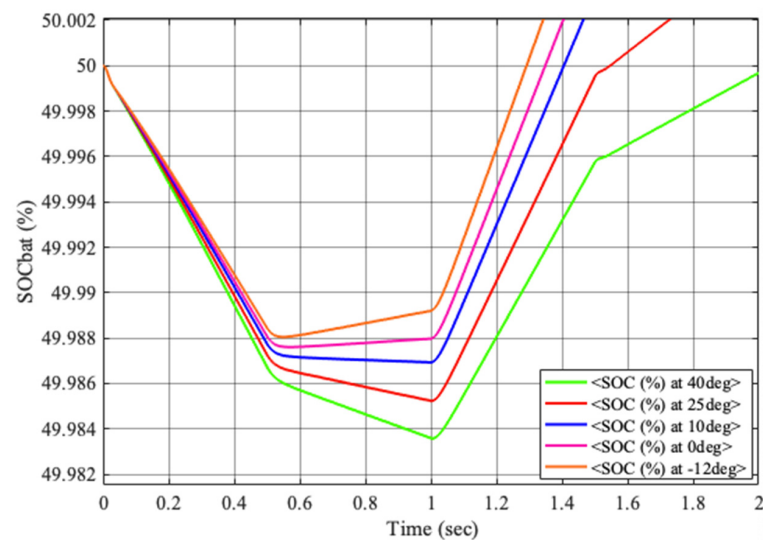


Figure 13. SOC_{bat} in the PV-HESS system using the TI controller for different temperatures.

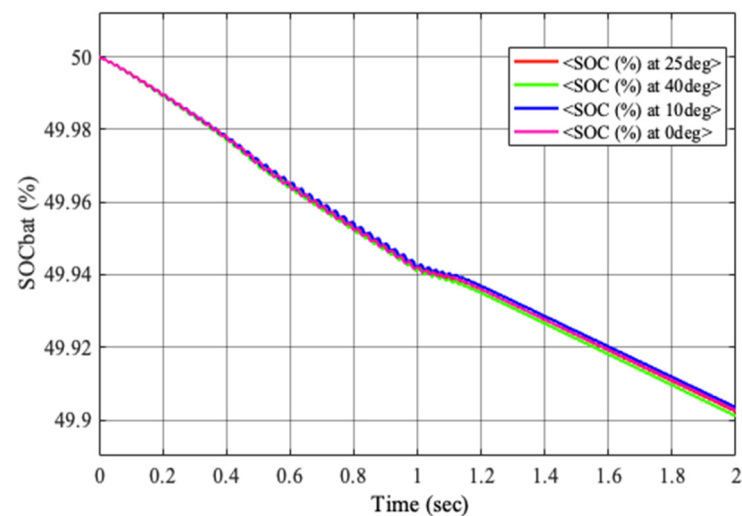


Figure 14. SOC_{bat} in a PV system without a supercapacitor.

5. Conclusions

In this paper, a combination battery and supercapacitor-based energy storage system, in a hybrid configuration, was investigated as backup to intermittent renewable energy sources such as solar PV for improving the system flexibility, stability, and reliability. An optimally tuned TI controller-based power management system was proposed for the DC bus voltage regulation. The controller was tuned using an efficient gradient free local search optimization technique (i.e., Nelder–Mead simplex search) by minimizing the time domain integral performance index (ITAE) taken as the cost function and the performance was also compared with the particle swarm global optimization technique. The efficacy of the proposed controller performance in terms of settling time, overshoot, rise time, and slew rate was analyzed and compared along with the FOPI and PI controllers. The investigation revealed that aside from a reduced oscillation in the DC bus response, the proposed control scheme was proven to be more robust and significantly outperformed the other controllers. Furthermore, by considering different operating scenarios such as variable irradiance, load, and temperature conditions, the performance and resilience of these controllers were investigated and compared to prove the effectiveness of the proposed method. An analysis of the SOC consumption of the battery with different values of temperature was carried out. The results indicate that the integration of a supercapacitor along with a battery reduced the battery SOC consumption by eliminating the peak currents, thereby improving the battery longevity and performance. Although the proposed TI controller-based scheme showed the optimum performance and adaptability for different conditions of the PV-HESS, further assessment and investigation need to be carried out based on different control strategies and optimization techniques. Enhanced performance analysis tests are required to detect more suitable techniques, giving better results.

Author Contributions: S.P.: Conceptualization, Methodology, Investigation, and Writing—Original draft preparation; M.R.K.: Conceptualization, Methodology, Supervision, Writing, Reviewing and Editing, and Validation; S.K.M.: Conceptualization, Methodology, Supervision, Writing, Reviewing and Editing, and Validation; S.P.G.: Conceptualization, Methodology, Investigation, Writing, Reviewing and Editing, Supervision, and Funding Acquisition; T.S.U., and B.A.: Supervision, Writing—Reviewing and Editing. All authors have read and agreed to the published version of the manuscript.

Funding: There was no funding available for this research.

Institutional Review Board Statement: Not applicable.

Informed Consent Statement: Not applicable.

Data Availability Statement: Not applicable.

Conflicts of Interest: The authors declare no conflict of interest.

References

1. Ustun, T.S.; Hashimoto, J.; Otani, K. Impact of Smart Inverters on Feeder Hosting Capacity of Distribution Networks. *IEEE Access* **2019**, *7*, 163526–163536. [[CrossRef](#)]
2. Singh, N.K.; Koley, C.; Gope, S.; Dawn, S.; Ustun, T.S. An Economic Risk Analysis in Wind and Pumped Hydro Energy Storage Integrated Power System Using Meta-Heuristic Algorithm. *Sustainability* **2021**, *13*, 13542. [[CrossRef](#)]
3. Zaheeruddin; Munish, M. Renewable energy management through microgrid central controller design: An approach to integrate solar, wind and biomass with battery. *Energy Rep.* **2015**, *1*, 156–163. [[CrossRef](#)]
4. Dey, P.P.; Das, D.C.; Latif, A.; Hussain, S.M.S.; Ustun, T.S. Active Power Management of Virtual Power Plant under Penetration of Central Receiver Solar Thermal-Wind Using Butterfly Optimization Technique. *Sustainability* **2020**, *12*, 6979. [[CrossRef](#)]
5. Latif, A.; Hussain, S.S.; Das, D.C.; Ustun, T.S. Double stage controller optimization for load frequency stabilization in hybrid wind-ocean wave energy based maritime microgrid system. *Appl. Energy* **2021**, *282*, 116171. [[CrossRef](#)]
6. Barbour, E.; Grant Wilson, I.A.; Radcliffe, J.; Ding, Y.; Li, Y. A review of pumped hydro energy storage development in significant international electricity markets. *Renew. Sustain. Energy Rev.* **2016**, *61*, 421–432. [[CrossRef](#)]
7. Cengiz, M.S.; Mamiş, M.S. Price-efficiency relationship for photovoltaic systems on a global basis. *Int. J. Photoenergy* **2015**, *2015*, 256101. [[CrossRef](#)]
8. Ustun, T.S.; Aoto, Y.; Hashimoto, J.; Otani, K. Optimal PV-INV Capacity Ratio for Residential Smart Inverters Operating Under Different Control Modes. *IEEE Access* **2020**, *8*, 116078–116089. [[CrossRef](#)]
9. Nadeem, F.; Hussain, S.M.S.; Tiwari, P.K.; Goswami, A.K.; Ustun, T.S. Review of Smart and Innovative Energy Storage Systems. In Proceedings of the International Conference on Vision Towards Emerging Trends in Communication and Networking (ViTECoN), Vellore, India, 30–31 March 2019; pp. 1–6.
10. Diouf, B.; Pode, R. Potential of lithium-ion batteries in renewable energy. *Renew. Energy* **2015**, *76*, 375–380.
11. Filomeno, M.V.; Pedro, S.M.; Anibal, T.A. Energy storage system for self-consumption of photovoltaic energy in residential zero energy buildings. *Renew. Energy* **2017**, *103*, 308–320.
12. Singh, S.; Chauhan, P.; Aftab, M.A.; Ali, I.; Hussain, S.M.S.; Ustun, T.S. Cost Optimization of a Stand-Alone Hybrid Energy System with Fuel Cell and PV. *Energies* **2020**, *13*, 1295. [[CrossRef](#)]
13. Latif, A.; Hussain, S.M.S.; Das, D.C.; Ustun, T.S. Design and Implementation of Maiden Dual-Level Controller for Ameliorating Frequency Control in a Hybrid Microgrid. *Energies* **2021**, *14*, 2418. [[CrossRef](#)]
14. Latif, A.; Hussain, S.M.S.; Das, D.C.; Ustun, T.S. Optimization of Two-Stage IPD-(1+I) Controllers for Frequency Regulation of Sustainable Energy Based Hybrid Microgrid Network. *Electronics* **2021**, *10*, 919. [[CrossRef](#)]
15. Kollimalla, S.K.; Mishra, M.K.; Narasamma, N.L. Design and analysis of novel control strategy for battery and supercapacitor storage system. *IEEE Trans. Sustain. Energy* **2014**, *5*, 1137–1144. [[CrossRef](#)]
16. Pattnaik, S.; Kumar, M.R.; Mishra, S.K. Supercapacitor-based automated fast charging system for electric vehicles. In *Symposium on Communication and Control for Robotic System*; Springer: Berlin, Germany, 2021; Volume 229, pp. 377–393.
17. Pattnaik, S.; Kumar, M.R.; Mishra, S.K.; Gautam, S.P. A review on characterization of supercapacitors and its efficiency analysis for different charging methods and applications. *Energy Storage* **2022**, e398. [[CrossRef](#)]
18. Niyigena, D.; Habineza, C.; Ustun, T.S. Computer-based smart energy management system for rural health centers. In Proceedings of the 3rd International Renewable and Sustainable Energy Conference (IRSEC), Marrakech, Morocco, 10–13 December 2015; pp. 1–5.
19. Latif, A.; Hussain, S.M.S.; Das, D.C.; Ustun, T.S. Optimum Synthesis of a BOA Optimized Novel Dual-Stage $PI - (1 + ID)$ Controller for Frequency Response of a Microgrid. *Energies* **2020**, *13*, 3446. [[CrossRef](#)]
20. Ulutas, A.; Altas, I.H.; Onen, A.; Ustun, T.S. Neuro-Fuzzy-Based Model Predictive Energy Management for Grid Connected Microgrids. *Electronics* **2020**, *9*, 900. [[CrossRef](#)]
21. Javed, K.; Ashfaq, H.; Singh, R.; Hussain, S.M.S.; Ustun, T.S. Design and Performance Analysis of a Stand-alone PV System with Hybrid Energy Storage for Rural India. *Electronics* **2019**, *8*, 952. [[CrossRef](#)]
22. Guentri, H.; Allaoui, T.; Mekki, M.; Denai, M. Power management and control of a photovoltaic system with hybrid battery-supercapacitor energy storage based on heuristics methods. *J. Energy Storage* **2021**, *39*, 102578. [[CrossRef](#)]
23. Abdolrasol, M.G.M.; Hussain, S.M.S.; Ustun, T.S.; Sarker, M.R.; Hannan, M.A.; Mohamed, R.; Ali, J.A.; Mekhilef, S.; Milad, A. Artificial Neural Networks Based Optimization Techniques: A Review. *Electronics* **2021**, *10*, 2689. [[CrossRef](#)]
24. Zou, C.; Zhang, L.; Hu, X.; Wang, Z.; Wik, T.; Pecht, M. A review of fractional-order techniques applied to lithium-ion batteries, lead-acid batteries, and supercapacitors. *J. Power Sources* **2018**, *390*, 286–296. [[CrossRef](#)]
25. Rao, K.D.; Ghosh, S.; Das, S.; Kumar, M.R. Transient behavior modeling-based hysteresis-dependent energy estimation of ultracapacitor. *IEEE Trans. Instrum. Meas.* **2020**, *69*, 6455–6464.
26. Latif, A.; Hussain, S.S.; Das, D.C.; Ustun, T.S.; Iqbal, A. A review on fractional order (FO) controllers' optimization for load frequency stabilization in power networks. *Energy Rep.* **2021**, *7*, 4009–4021. [[CrossRef](#)]
27. Freeborn, T.J.; Maundy, B.; Elwakil, A.S. Fractional-order models of supercapacitors, batteries and fuel cells: A survey. *Mater. Renew. Sustain. Energy* **2015**, *4*, 9. [[CrossRef](#)]

28. Chen, Y.; Petras, I.; Xue, D. Fractional order control—A tutorial. In Proceedings of the 2009 American Control Conference, St. Louis, MO, USA, 10–12 June 2009; Volume 8, pp. 1397–1411.
29. Khokhar, B.; Dahiya, S.; Parmar, K.P.S. A novel hybrid fuzzy PD-TID controller for load frequency control of a standalone microgrid. *Arab. J. Sci. Eng.* **2021**, *46*, 1053–1065.
30. Guha, D.; Roy, P.; Banerjee, S. A maiden application of salp swarm algorithm optimized cascade tilt-integral-derivative controller for load frequency control of power systems. *IET Gener. Transm. Distrib.* **2019**, *13*, 1110–1120. [[CrossRef](#)]
31. Ahmed, B.; Abdelkrim, T.; Mordjaoui, M.; Mohcene, B.; Moussa, S. An optimal tilt integral derivative applied to the regulation of DC link voltage in a stand-alone hybrid energy system. *J. Eur. Syst. Autom.* **2021**, *54*, 607–616.
32. Mussadiq, U.; Kausar, T.; Ahmed, S.; Kim, S.M. A hybrid storage system for energy sharing and management within prosumers' community. In Proceedings of the 2022 5th International Conference on Energy Conservation and Efficiency, Lahore, Pakistan, 16–17 March 2022; pp. 1–6.
33. Keshan, H.; Thornburg, J.; Ustun, T.S. Comparison of lead-acid and lithium ion batteries for stationary storage in off-grid energy systems. In Proceedings of the 4th IET Clean Energy and Technology Conference (CEAT 2016), Kuala Lumpur, Malaysia, 14–15 November 2016.
34. Elgendy, M.A.; Zahawi, B.; Atkinson, D.J. Assessment of Perturb and Observe MPPT algorithm implementation techniques for PV pumping applications. *IEEE Trans. Sustain. Energy* **2012**, *3*, 21–33. [[CrossRef](#)]
35. Ustun, T.S.; Nakamura, Y.; Hashimoto, J.; Otani, K. Performance analysis of PV panels based on different technologies after two years of outdoor exposure in Fukushima, Japan. *Renew. Energy* **2019**, *136*, 159–178. [[CrossRef](#)]
36. Cabrane, Z.; Ouassaid, M.; Maaroufi, M. Management and control of storage photovoltaic energy using battery-supercapacitor combination. In Proceedings of the Second World Conference on Complex Systems (WCCS), Agadir, Morocco, 10–12 November 2014; pp. 380–385.
37. Bhatti, S.A.; Malik, S.A.; Daraz, A. Comparison of P-I and I-P controller by using Ziegler-Nichols tuning method for speed control of DC motor. In Proceedings of the 2016 International Conference on Intelligent Systems Engineering (ICISE), Islamabad, Pakistan, 15–17 January 2016; pp. 330–334. [[CrossRef](#)]
38. Kumar, M.R.; Ghosh, S. Hybrid Optimization Based FOPI Controller Design with Real-Time Validation. *IFAC Pap. Line* **2018**, *51*, 78–83. [[CrossRef](#)]
39. Kumar, M.R.; Deepak, V.; Ghosh, S. Fractional-order controller design in frequency domain using an improved nonlinear adaptive seeker optimization algorithm. *Turk. J. Electr. Eng. Comput. Sci.* **2017**, *25*, 4299–4310. [[CrossRef](#)]
40. Das, S. *Functional Fractional Calculus*; Springer Science and Business Media: Berlin, Germany, 2011.
41. Maria, C.A.; Christos, C.M.; Soteris, A.K.; Paul, C. A novel power management algorithm for a residential grid-connected PV system with battery-supercapacitor storage for increased self-consumption and self-sufficiency. *Energy Convers. Manag.* **2021**, *246*, 11467.
42. Pankaj, D.; Mukhija, P.; Saxena, A.R.; Yogendra, A. Comparative performance investigation of optimal controller for AGC of electric power generating systems. *Automatika* **2017**, *57*, 902–921.
43. Özdemir, M.; Öztürk, D. Comparative performance analysis of optimal PID parameters tuning based on the optics inspired optimization methods for automatic generation control. *Energies* **2017**, *10*, 2134. [[CrossRef](#)]
44. Mouayad, A.S.; Bestoun, S.A. A new multiobjective performance criterion used in PID tuning optimization algorithms. *J. Adv. Res.* **2016**, *7*, 125–134.
45. Lagarias, J.C.; Reeds, J.A.; Wright, M.H.; Wright, P.E. Convergence properties of the Nelder–Mead simplex method in low dimensions. *SIAM J. Optim.* **1998**, *9*, 112–147. [[CrossRef](#)]
46. Ahmed, Z.; Atlas, M. Optimal solution of integro-differential Equation of Suspension Bridge Model using Genetic Algorithm and Nelder-Mead method. *J. Assoc. Arab. Univ. Basic Appl. Sci.* **2017**, *24*, 310–314.
47. Chen, P.L.; Yang, M.C.; Sun, T.Y. PSO-based on-line tuning PID controller for setpoint changes and load disturbance. In Proceedings of the 2011 IEEE Congress of Evolutionary Computation (CEC), New Orleans, LA, USA, 5–8 June 2011; pp. 1887–1894. [[CrossRef](#)]